Journal of Physics C: Solid State Physics

Infra-red absorption of beryllium in cadmium telluride: II

To cite this article: C T Sennett *et al* 1969 *J. Phys. C: Solid State Phys.* **2** 1137

J. PHYS. C (SOLID ST. PHYS.), 1969, SER. 2, VOL. 2. PRINTED IN GREAT BRITAIN

Infra-red absorption of beryllium in cadmium telluride: II

C. T. SENNETT†, D. R. BOSOMWORTH‡, W. HAYES‡, and A. R. L. SPRAY§

† Royal Radar Establishment, Malvern

‡ R.C.A. Laboratories, Princeton, New Jersey, U.S.A.

§ Clarendon Laboratory, University of Oxford

MS. received 3rd January 1969

Abstract. The dispersion curves and normal modes of vibration of CdTe have been calculated using a shell model. The single-phonon and combined two-phonon density of states have been computed and the latter is compared with measured two-phonon infra-red absorption. The infra-red absorption induced in CdTe by Be impurity is also calculated and compared with experiment. A resonance mode of Be is observed at 61 cm^{-1} and a local mode at 391 cm^{-1}; calculated values of these modes obtained using a defect mass approximation are in good agreement with experiment. The structure of observed side bands arising from a simultaneous excitation of the local Be mode and lattice band modes is discussed.

1. Introduction

In the previous paper (Hayes and Spray 1969, henceforth referred to as I) we have given a detailed description of the properties of the localized vibrational mode of Be in CdTe. In the present paper we describe a resonant mode of Be in CdTe which occurs at 61 cm^{-1} and also the side-band structure on the fundamental of the local mode (see also I). The side-band structure arises from the simultaneous excitation of one local mode and one lattice phonon and gives detailed information about lattice phonons. This information is particularly valuable in the case of CdTe because the large neutron cross section of Cd isotopes makes neutron diffraction experiments on CdTe impracticable.

In order to predict the Be induced infra-red absorption in CdTe we have calculated the dispersion curves and normal modes of vibration for CdTe. We have obtained the Green functions for the unperturbed lattice and, using the defect mass approximation, we obtain quite good agreement between the calculated and measured values for the resonant and local mode of Be.

Our measurements on CdTe : Be in the region 20–120 cm^{-1} were made with an evacuated interferometric spectrometer. This was used with a carbon bolometer detector cooled to 1·5 °K. Measurements at higher energies were made with a grating monochromator (see I).

2. Experimental results

The absorption of CdTe containing 300 p.p.m. by weight of Be ions in the region 20–120 cm^{-1} is shown in figure 1. The sharp line at 61·0 cm^{-1} is found only in the doped crystals. With the exception of this line the absorption of undoped CdTe in this region is similar to that shown in the figure. It will be shown later (see § 3) that the 61 cm^{-1} line is a resonant mode of Be and that its sharpness is due to the low density of states near this frequency; it may also be described as a quasi-local mode. The peaks at 71·5, 94 and 104 cm^{-1} observed at 1·8 °K (see figure 1) are due to two-phonon summation bands of the host crystal (see § 3 and § 5). The crystal absorption in this region at 78 °K becomes intense (figure 1, curve B) owing to the excitation of summation and difference bands.

Some properties of the side-band structure on the high-energy side of the local mode of the fundamental (figure 2) have already been described in I. These transitions arise from simultaneous excitation of local mode and a lattice band mode. The side bands represent a modified single-phonon density of states (see § 3 and § 5) for CdTe. The 61 cm^{-1} peak in the side-band structure is due to the simultaneous excitation of the local

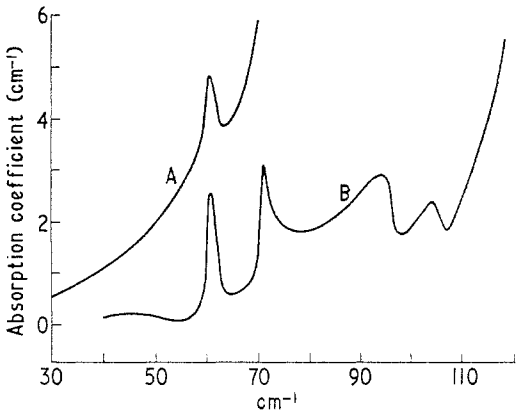

Figure 1. Infra-red absorption of CdTe:Be A at 1·8 °K and B at 78 °K.

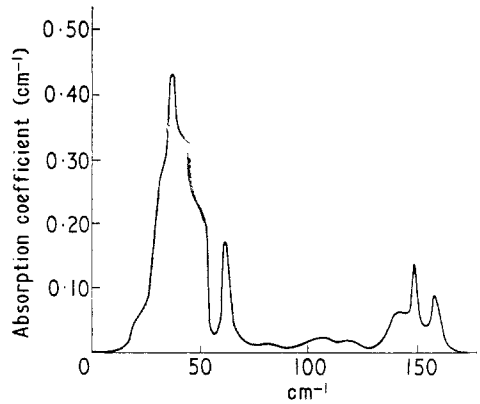

Figure 2. Experimentally determined side-band structure on the high-energy side of the fundamental of the local vibrational mode of Be in CdTe at 4 °K. The zero of the energy scale coincides with the peak of the local-mode line.

mode and the 61 cm^{-1} resonance mode of Be. The side-band structure is too weak to enable us to investigate in detail the anti-Stokes component on the low-energy side of the local-mode fundamental or side bands on higher harmonics (see I).

The two-phonon summation bands of CdTe on the high-energy side of the restrahl band have been described by other authors (Bottger and Geddes 1967, Stafsudd *et al.* 1967). We give a calculated two-phonon combined density of states, for comparison, in § 3.

3. Calculation of the vibrational dispersion curves for CdTe

A shell-model calculation was used to obtain the dispersion curves for CdTe. Table 1 contains some physical properties which were used in the shell-model calculation and which partly describe the macroscopic behaviour of the system. Because of the nature of the

Table 1. Some physical constants of CdTe

Constant	Reference
$\omega_{LO} = 171{\cdot}4\ cm^{-1}$	Halsted *et al.* (1961)
$\omega_{TO} = 140\ cm^{-1}$	Mears *et al.* (1968)
$\epsilon_0 = 10{\cdot}60$	Marple (1964)
$\epsilon_\infty = 7{\cdot}05$	
$c_{11} = 5{\cdot}351 \times 10^{11}\ dyn\ cm^{-2}$	McSkimm and Thomas (1962)
$c_{12} = 2{\cdot}681 \times 10^{11}\ dyn\ cm^{-2}$	
$c_{44} = 1{\cdot}994 \times 10^{11}\ dyn\ cm^{-2}$	

input data we expect that only the long-wave region of the dispersion curves will be accurately described. The relation (Lyddane *et al.* 1941)

$$\left(\frac{\epsilon_0}{\epsilon_\infty}\right)^{1/2} = \left(\frac{\nu_{LO}}{\nu_{TO}}\right)_{k=0}$$

was used to obtain the value of ν_{TO} given in table 1, which therefore contains six independent parameters. We restrict the number of adjustable parameters in our calculation to six

and, although this implies a considerable degree of approximation, the calculation is sufficiently accurate to interpret the main features of our spectra.

Solving for six non-linear equations to fit six parameters can lead to more than one solution and can take a long time. For this reason the problem is divided into a number of steps using a succession of restricted approximations with a number of adjustable parameters smaller than six. The output of each step is used as a starting value for the next less restrictive approximation. Each approximation corresponds to some (possibly unrealistic) assumption as to the nature of the forces, so the whole process is physically interesting as well as being convenient for calculation. The effect of the various assumptions will be described in terms of the size of the calculated effective charge.

The form of the dynamical matrix, divided into short-range and long-range parts, has been given by a number of authors (e.g. Dolling and Waugh 1963, Cowley 1962) together with expressions for the macroscopic physical quantities (table 1). The actual numerical details of all the calculations may be obtained from one of the authors (C.T.S.). The first step in finding a set of input parameters was to assume a rigid-ion nearest-neighbour model and to fit the central force constant and effective charge to ω_{TO} and ω_{LO}. When this is done the effective charge is found to be 0·9 but the calculated elastic constants are 25% too small for c_{11} and negative for c_{44}. Under certain assumptions about the force constants it has been shown by Cowley that, using the shell model, the elastic constants may be written in terms of the core: core force constants and the dielectric constants only. This assumption was used as the next step and the nearest-neighbour force constants and effective charge were fitted to the elastic constants using the experimental value of the static dielectric constant. This fitting had an exact solution with an effective charge of 2·3 and an approximate solution with a very small effective charge. The first of these was rejected as the calculated value of c_{44} was negative.

The next step was to assume that the ions possessed equal polarizabilities and the effective charge Z for CdTe is then determined by the dielectric constants and ω_{TO} as

$$|Z| = \frac{3\omega_{TO}}{(\epsilon_\infty+2)e}\left\{\frac{\mu(\epsilon_0-\epsilon_\infty)v}{4\pi}\right\}^{1/2} = 0{\cdot}8. \tag{1}$$

This formula may be derived from the shell-model equations of motion by making the equal polarizability assumption. The reduced mass is μ and the cell volume is v. With this value of Z the elastic constant c_{44} is always negative for reasonable values of the force constants. On the other hand, if second-neighbour central forces are introduced, an approximate solution may be obtained and this was also rejected because this second-neighbour force becomes as large as the nearest-neighbour force.

Accordingly, it was assumed that the cadmium ions are not polarizable and this assumption allows four parameters to be fitted to ω_{TO}, ω_{LO}, ϵ_∞ and c_{11}. In this case, with nearest-neighbour forces, the effective charge becomes 0·6 and there is a 20% mismatch to c_{12} and c_{44}. Introducing a central second-neighbour force allows an approximate match to all six constants with an effective charge of 0·02. This approximate match may be made exact by fixing the nearest-neighbour central force at the value which gives the approximate match and introducing a non-central component in the second-neighbour forces. This model (model I) was used for the initial calculation and the single-phonon density of states $S(\omega)$ for the model is shown in figure 3.

Model I makes the assumption that shell-core interactions are proportional to core–core interactions or, in the notation of Dolling and Waugh, $\gamma_T = \gamma_R$. For reasons which will be explained later a further calculation was made fixing the TA frequency at the zone edge (X) at 50 cm^{-1} and this was achieved by varying γ_T. This variation leaves the fit to the other parameters undisturbed because the core–shell interaction does not effect the macroscopic quantities. The single-phonon density of states $S(\omega)$ for this model (model II) is shown in figure 4(*a*), and a weighted density of states $S(\omega)/\omega^2$ is shown in figure 4(*b*) (see § 5). It is hoped that this explanation of the steps which were taken to fit the experimental results will justify to some extent the somewhat arbitrary choice of model.

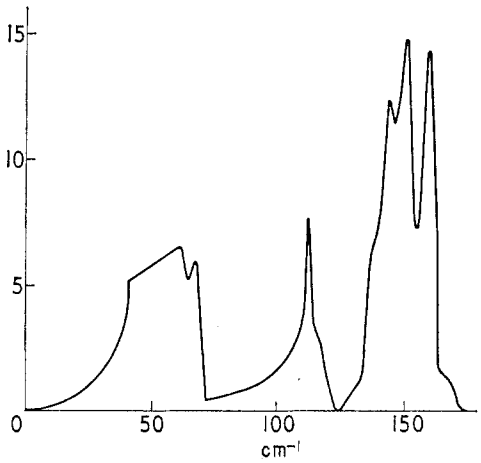

Figure 3. Single-phonon density of states $S(\omega)$ for model I. The ordinate is arbitrary.

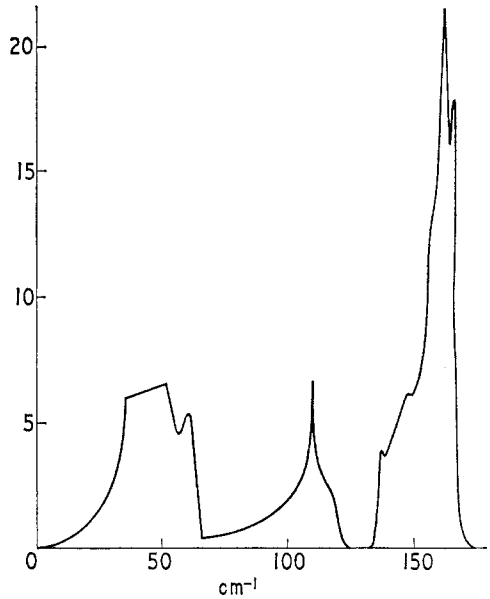

Figure 4(*a*). Single-phonon density of states $S(\omega)$ for model II. The ordinate is arbitrary.

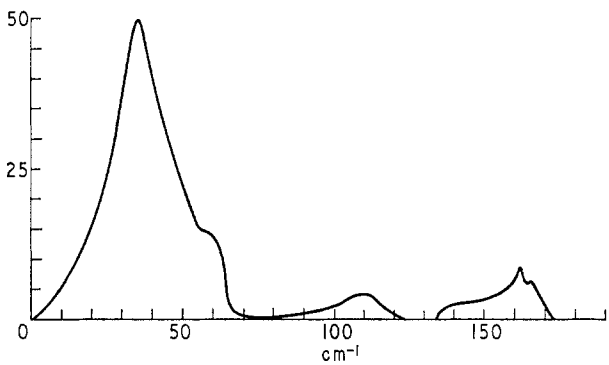

Figure 4(*b*). $S(\omega)/\omega^2$ for model II. The ordinate is arbitrary.

The two density of states curves (figures 3, 4(*a*)) were obtained by an extrapolation procedure similar to that proposed by Gilat and Dolling (1964) and correspond to one million extrapolated points in the Brillouin zone. The force constants for model II in the notation of Dolling and Waugh (1963) are given in table 2, and the dispersion curves are shown in

Table 2. Shell-model parameters for CdTe (model II)†

α_R	$\gamma_R = \gamma_S$	π_2	d_2	S_R	γ_T
8·16	0·77	0·159	0·833	0·0	0·188
Z	λ	μ	ν	δ	
0·041	0·25	−0·13	0·39	0·0	

† See Dolling and Waugh (1963) for definition of parameters and for units.

figure 5. The two-phonon combined density of states, including overtones, is plotted in figure 6 for model II.

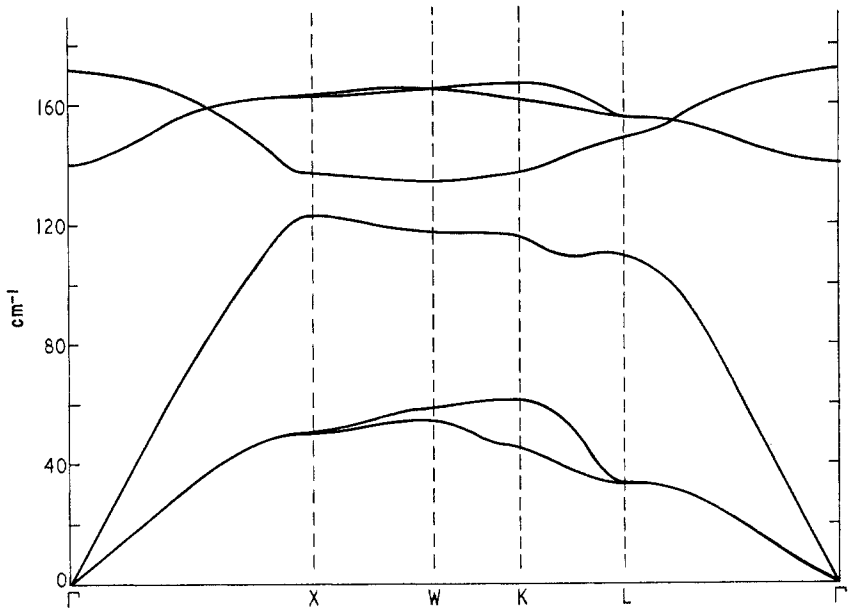

Figure 5. Dispersion curves of CdTe for model II.

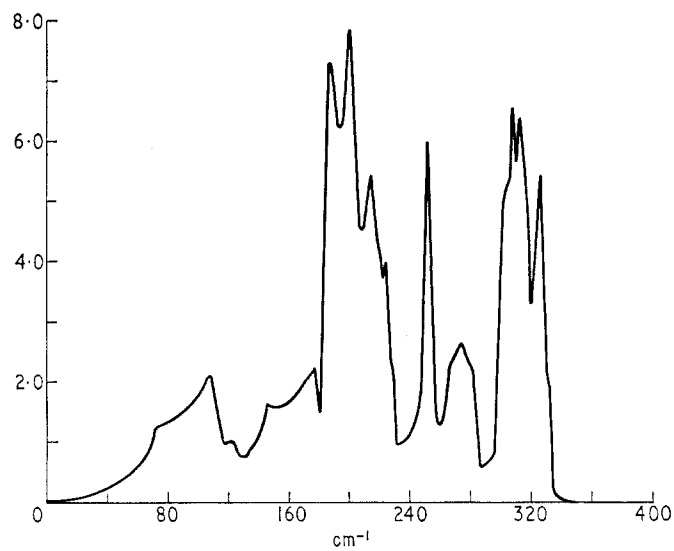

Figure 6. Combined density of states for model II. The ordinate is arbitrary.

4. Calculation of the effect of doping

It was assumed that the Be forms a substitutional impurity on a cadmium site. In view of the approximate nature of the calculation it was felt that it would be unrealistic to treat the Be as anything other than an isotopic impurity. This is in any case likely to reproduce the main features of the spectrum as the mass change is so large its effect will be expected to outweigh that of any force-constant change, and will result in a highly localized mode. This assumption considerably simplifies the computation since the only component of the Green function it is necessary to calculate is

$$g_{x1x1}(0, 0; \omega) = \sum_{j,y} \frac{|\sigma_{x1}{}^{j}(\mathrm{y})|^2}{NM_1\{\omega^2 - \omega_j{}^2(\mathrm{y})\}} \tag{2}$$

in the notation of Elliott *et al.* (1965); the cadmium site is taken as 1. The summand was calculated in a simple way using a random sample of 9000 points in reciprocal space and summing over the star of wave vectors at each point. The principal part of this function, for model II, is plotted against ω in figure 7. On the same graph the function $(\epsilon M\omega^2)^{-1}$ is also plotted, where ϵ is the mass defect parameter (Elliott *et al.*); the intersection of these curves, for $\omega > \omega_{\max}$, gives the frequency of the localized mode (Elliott *et al.*). This frequency (not shown on figure 7) is 417 cm^{-1}, to be compared with the experimental value of 391 cm^{-1} at 4 °K (see I). The agreement is rather better than might be expected. As the masses of cadmium and tellurium are very similar, this approximation is not able to distinguish between substitutional impurities at either site. For Be on a tellurium site the calculated local-mode frequency is 399 cm^{-1}, and both results agree with the experimental observations to within the accuracy of the calculation. However, on chemical grounds, we expect Be to dissolve in cadmium sites (see also I).

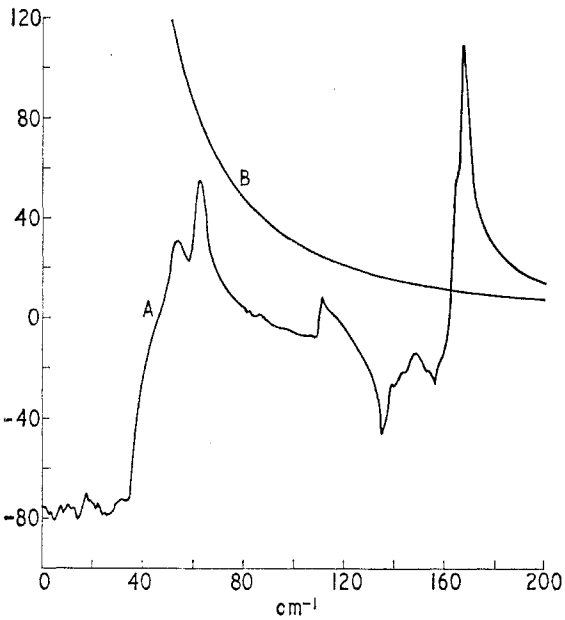

Figure 7. A: Principal part of the Green function (equation (2), text). B: mass defect parameter $(\epsilon M\omega^2)^{-1}$, as a function of ω. The ordinate is arbitrary.

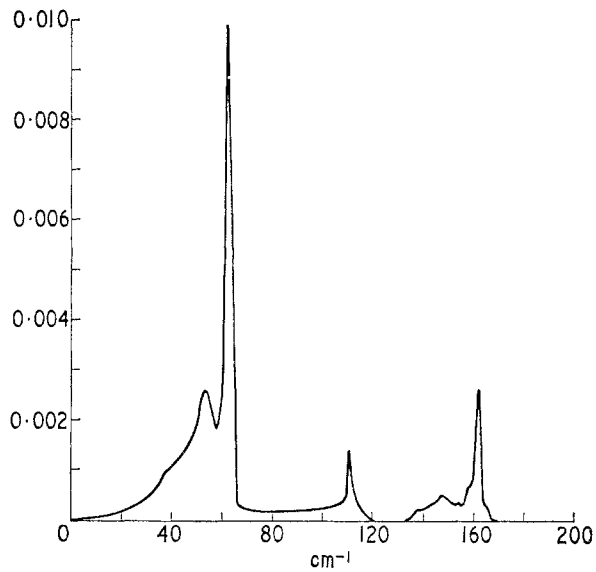

Figure 8. Mean-square vibrational amplitude at the defect site (equation (3), text). The ordinate is arbitrary.

The defect-induced absorption in the band-mode region and the side-band structure on the local mode are much more difficult to calculate since they depend upon the manner in which radiation couples to the defect. Also, because they are largely the result of vibrations occurring within the band of unperturbed frequencies they are much more sensitive to the details of the lattice dynamical model. The matrix of the coupling is largely a matter for conjecture and the model is approximate, so no calculations were performed taking into account either the motion of the neighbouring atoms or the effect of changing the polarizability. Instead, it was assumed that the impurity-induced absorption was proportional to the amplitude of the vibrations at the defect site. It is probable that this is an important factor in the side-band absorption also (see § 5). The mean square amplitude is given by the equation

$$\chi_x(\omega) = \frac{F_{xx}(\omega)}{\{1 - M\epsilon\omega^2 g_{xx}(0, 0; \omega)\}^2 + \frac{1}{4}\pi^2 M^2\epsilon^2\omega^2 F_{xx}(\omega)} \tag{3}$$

and this is plotted for model II in figure 8. The function F is determined by the amplitude squared of the eigenvectors, summed over the star of the wave vector, $\boldsymbol{k}$, and evaluated as a function of frequency (Elliott *et al.*).

5. Discussion

The most pronounced feature of the calculated Be-induced absorption (figure 8) is the sharp peak at 61 cm^{-1}. This is a resonance (or quasi-local) mode in which the Be has a large amplitude of vibration owing to the sharp fall-off in the TA density of states near this frequency (figure 4(*a*)) and is a consequence of the near coincidence, at this frequency, of A and B in figure 7. This fall-off is a characteristic of many compounds of the zinc-blende structure which have anomalously low TA branches (see Dolling and Waugh). With model I, which had a higher TA cut-off frequency (figure 3), the resonance appeared at 68 cm^{-1}. A second resonance appears at 162 cm^{-1} (figure 7, 8) but the position of this peak is likely to be more sensitive to the details of the calculation. Other weak peaks in figure 8 are due to peaks in the single-phonon density of states (figure 4(*a*)). The P2 discontinuity at 118 cm^{-1} which is due to LA at W (W_1 symmetry) does not appear in the calculated defect-induced absorption (figure 8). Also, the P3 discontinuity due to X_1 at 117·5 cm^{-1} (figure 4(*a*)) does not appear in figure 8. These results are in agreement with the symmetry arguments of Loudon (1964).

From measurements on doped and undoped crystals it is apparent that the only impurity-induced absorption observed in the 20–120 cm^{-1} range is the peak at 61 cm^{-1} (figure 1). This is in agreement with calculation (figure 8) which suggests that the additional impurity-induced absorption in this range would be too weak to be observed. It is likely that the TA contribution would be even less than that indicated in figure 8 since the acoustic modes, although having a large amplitude at the defect site, are still relatively unperturbed by the small defect and have a small dipole moment. The impurity-induced absorption at 162 cm^{-1} will, of course, be overlaid by restrahl absorption and will not be observable.

The side-band structure in the present case can be accounted for by cubic anharmonicity (see I) and is determined by the product of an in-band displacement and a local-mode displacement. If the major contribution to this process occurs when both displacements are on the defect site the side-band structure would be given by figure 8, modified by an energy denominator. However, it is likely that the largest contribution to the side-band structure comes from local-mode displacements coupled to in-band displacements on nearest neighbours. The resonance modes at 61 and 162 cm^{-1} will therefore be considerably reduced in intensity in the side-bands relative to the band modes, as observed (see figure 2 and below). The measured displacement of the side-band peak at 61 cm^{-1} from the local mode is the same as the measured energy of the resonant mode although small differences may be expected to occur (see Bäuerle and Fritz 1968).

In the present case there are no symmetry restrictions on band phonons in the side-band structure (see Loudon 1964). An approximation in which the shape function for the band-mode contribution to the side bands is given by $S(\omega)/\omega^3$ has been used by Timusk and Klein (1966). Using the Debye approximation, Elliott *et al.* found that the shape function for the band-mode contribution to the side bands is given by $S(\omega)/\omega$. However, the Debye approximation is not likely to be good at the zone boundary where the phonons which determine the side-band structure largely occur. The actual situation in the present case appears to be intermediate between these approximations. In figure 4(*b*) we have plotted $S(\omega)/\omega^2$ using our calculated $S(\omega)$ (figure 4(*a*)) and comparison with figure 2 indicates that the best agreement between the experimentally determined side-band shape and calculation would be obtained with an exponent of ω in the shape function slightly less than 2.

Comparison of figures 2 and 4(*b*) shows that the optical-mode contribution to the side bands is correctly placed. It is possible that the resonance placed at 162 cm^{-1} in the calculation (figure 8) may contribute to the observed structure (figure 2). Figure 4(*b*) will not, of course, be expected to agree with figure 2 in the vicinity of 60 cm^{-1} where a resonance occurs (figure 8). In general, however, the shape of the TA contribution to the side bands (figure 2) approximates reasonably well to the TA band in figure 4(*b*). However, the

calculated contribution is larger than observed in the region 0–20 cm^{-1} (figure 2); experimentally this is a region difficult to measure with precision because of its closeness to the local mode. Comparison of our calculated and observed local-mode frequency (§ 4) suggests that a reduction of force constants at the Be site of the order of 10% may be occurring and this would enhance the calculated contribution of the lower mode frequencies to the side-band structure (see e.g. Timusk and Klein).

The intrinsic lattice absorption, apart from the restrahl band, arises from combinations and overtones of the unperturbed lattice bands. The first observed peak at 71·5 cm^{-1} (figure 1) occurs in the same position as a calculated overtone of the TA phonons at L where there is a P1-type discontinuity (figure 6). A similar discontinuity at X (at 100 cm^{-1}) is obscured by the rapidly rising intensity of the combination bands which peaks at 109 cm^{-1} (figure 6). This peak is followed by another at 120 cm^{-1} due to overtones in the X–K TA branches which fall in a trough in the combined density of states (figure 6). Experimentally (figure 2) the L peak is sharper than predicted and the observed peaks in the 90–110 cm^{-1} range are at an energy lower than predicted. It seems worth mentioning that a donor with an ionization energy of 85 cm^{-1} has been observed in CdTe by electrical methods (Segall *et al.* 1963, Mears *et al.* 1968) but this should not affect the infra-red absorption in our highly resistive crystals.

The structure in the intrinsic absorption at energies higher than the restrahl energy is broad (Bottger and Geddes 1967, Stafsudd *et al.* 1967) and does not show the critical point detail in our calculation (figure 6). We shall not therefore attempt an interpretation in terms of individual phonons but we point out that there are five major regions in our combined density of states curve:

TA+TA	TA+LA	TA+O LA+LA	LA+O	O+O
0–120	120–180	180–230	230–280	280–340 cm^{-1}

and these correlate quite well with the observed intrinsic absorption.

In conclusion we point out that observations of Be-doped CdTe have enabled us to obtain a lattice dynamical model of CdTe which gives phonon frequencies in the acoustic region to an accuracy of about 5 cm^{-1} and in the optical region to an accuracy of about 10 cm^{-1}. Although approximate, the model enables us to identify most features of the impurity-induced absorption and should be useful for the interpretation of other measurements in CdTe (see e.g. Balkanski, *et al.* 1968).

Acknowledgments

One of us (A.R.L.S.) is indebted to the Rhodes Trust for the award of a Scholarship.

References

Balkanski, M., Beserman, R., and Vodopianov, L. K., 1968, *Localised Excitations in Solids*, Ed. R. F. Wallis (New York: Plenum), p. 154.

Bäuerle, D., and Fritz, B., 1968, *Phys. St. Solidi*, **29**, 639.

Bottger, G. L., and Geddes, A. L., 1967, *J. Chem. Phys.*, **47**, 4858.

Cowley, R. A., 1962, *Proc. R. Soc.* A, **268**, 121.

Dolling, G., and Waugh, J. L. T., 1963, *Lattice Dynamics*, Ed. R. F. Willis (Oxford: Pergamon), p. 19.

Elliott, R. J., Hayes, W., Jones, G. D., MacDonald, H. F., and Sennett, C. T., 1965, *Proc. R. Soc.* A, **289**, 1.

Gilat, G., and Dolling, G., 1964, *Phys. Lett*, **8**, 304.

Halsted, R. E., Lorenz, M. R., and Segall, B., 1961, *J. Phys. Chem. Solids*, **22**, 109.

Hayes, W., and Spray, A. R. L., 1969, *J. Phys.* C (*Solid St. Phys.*), [2], **2**, 1129–36.

Loudon, R., 1964, *Proc. Phys. Soc.*, **84**, 379.

Lyddane, R. H., Sachs, R. G., and Teller, E., 1941, *Phys. Rev.*, **59**, 673.

Marple, D. T. F., 1964, *J. Appl. Phys.*, **35**, 539.

McSkimm, H. J., and Thomas, D. G., 1962, *J. Appl. Phys.*, **33**, 56.
Mears, A. L., Spray, A. R. L., and Stradling, R. A., 1968, *J. Phys.* C (*Proc. Phys. Soc.*), [2], **1**, 1412.
Segall, B., Lorenz, M. R., and Halsted, R. E., 1963, *Phys. Rev.*, **129**, 2471.
Stafsudd, O. M., Haak, F. A., and Radisavljevic, K., 1967, *J. Opt. Soc. Am.*, **57**, 1475.
Timusk, T., and Klein, M. V., 1966, *Phys. Rev.*, **141**, 664.